Chemical Science

ROYAL SOCIETY OF CHEMISTRY

EDGE ARTICLE

View Article Online
View Journal | View Issue

Cite this: *Chem. Sci.*, 2021, **12**, 2986

All publication charges for this article have been paid for by the Royal Society of Chemistry

Encapsulation of tricopper cluster in a synthetic cryptand enables facile redox processes from $Cu^{I}Cu^{I}Cu^{I}$ to $Cu^{II}Cu^{II}Cu^{II}$ states†

Weiyao Zhang, Curtis E. Moore and Shiyu Zhang *

One-pot reaction of tris(2-aminoethyl)amine (TREN), $[Cu^{I}(MeCN)_4]PF_6$, and paraformaldehyde affords a mixed-valent $[\mathbf{TREN_4}Cu^{II}Cu^{I}Cu^{I}(\mu_3\text{-}OH)](PF_6)_3$ complex. The macrocyclic azacryptand $\mathbf{TREN_4}$ contains four TREN motifs, three of which provide a bowl-shape binding pocket for the $[Cu_3(\mu_3\text{-}OH)]^{3+}$ core. The fourth TREN caps on top of the tricopper cluster to form a cryptand, imposing conformational constraints and preventing solvent interaction. Contrasting the limited redox capability of synthetic tricopper complexes reported so far, $[\mathbf{TREN_4}Cu^{II}Cu^{I}Cu^{I}(\mu_3\text{-}OH)](PF_6)_3$ exhibits several reversible single-electron redox events. The distinct electrochemical behaviors of $[\mathbf{TREN_4}Cu^{II}Cu^{I}Cu^{I}(\mu_3\text{-}OH)](PF_6)_3$ and its solvent-exposed analog $[\mathbf{TREN_3}Cu^{II}Cu^{II}Cu^{II}(\mu_3\text{-}O)](PF_6)_4$ suggest that isolation of tricopper core in a cryptand enables facile electron transfer, allowing potential application of synthetic tricopper complexes as redox catalysts. Indeed, the fully reduced $[\mathbf{TREN_4}Cu^{I}Cu^{I}Cu^{I}(\mu_3\text{-}OH)](PF_6)_2$ can reduce O_2 under acidic conditions. The geometric constraints provided by the cryptand are reminiscent of Nature's multicopper oxidases (MCOs). For the first time, a synthetic tricopper cluster was isolated and fully characterized at $Cu^{I}Cu^{I}Cu^{I}$ (**4a**), $Cu^{II}Cu^{I}Cu^{I}$ (**4b**), and $Cu^{II}Cu^{II}Cu^{I}$ (**4c**) states, providing structural and spectroscopic models for many intermediates in MCOs. Fast electron transfer rates (10^5 to 10^6 M^{-1} s^{-1}) were observed for both $Cu^{I}Cu^{I}Cu^{I}/Cu^{II}Cu^{I}Cu^{I}$ and $Cu^{II}Cu^{I}Cu^{I}/Cu^{II}Cu^{II}Cu^{I}$ redox couples, approaching the rapid electron transfer rates of copper sites in MCO.

Received 1st October 2020
Accepted 24th December 2020

DOI: 10.1039/d0sc05441k

rsc.li/chemical-science

Introduction

Synthetic tricopper clusters have been a prominent synthetic target for the (bio)inorganic community over the past few decades,[1–9] since tricopper centers were identified/proposed as essential active sites for biological reduction of O_2 to H_2O in multicopper oxidase (MCO)[10,11] and aerobic hydroxylation of methane in particulate methane monooxygenase (pMMO).[12] Although a tricopper active site in pMMO has been disputed, the conversion of methane to methanol was demonstrated with small-molecule tricopper complexes.[13,14] In both oxygen reduction and hydrocarbon hydroxylation, the synergy of three Cu^{II}/Cu^{I} redox couples in tricopper clusters is essential to harness the oxidative power of O_2. Therefore, understanding factors governing the redox of tricopper clusters as a single unit is fundamental to their development as biomimetic catalysts in fuel cell technology and functionalization of alkanes.

An ideal tricopper redox catalyst should be able to engage all three Cu^{II}/Cu^{I} couple and accommodate four redox states from $Cu^{I}Cu^{I}Cu^{I}$ to $Cu^{II}Cu^{II}Cu^{II}$. However, the majority of synthetic tricopper clusters reported to date have limited redox capability, and only isolated at a single oxidation state (primarily $Cu^{II}Cu^{II}Cu^{II}$ or $Cu^{I}Cu^{I}Cu^{I}$).[15,16] Copper(I) center (d^{10}) and copper(II) center (d^{9}) prefer distinct geometry due to the Jahn–Teller effect. The redox of Cu^{II}/Cu^{I}, in an unconstrained solvent-exposed environment, often results in significant geometric rearrangement associated with high reorganization energy.[17] Notably, among *ca.* 186 crystallographically characterized molecular tricopper μ_3-E, (E = O, OH, S) clusters, **1** and **2** (Fig. 1A and B) represents the only two redox-active examples.[18,19] Even **1** and **2**, however, cannot be further reduced to the $Cu^{I}Cu^{I}Cu^{I}$ state,[16] which is crucial for the activation of O_2 during catalytic oxygen reduction reaction (ORR) and hydrocarbon hydroxylation. In sharp contrast, Nature's trinuclear copper cluster (TNC) in MCOs has been observed in three different oxidation states: fully reduced ($Cu^{I}Cu^{I}Cu^{I}$, FR), alternative resting ($Cu^{II}Cu^{I}Cu^{I}$, AR), and native intermediate ($Cu^{II}Cu^{II}Cu^{II}$, NI). Unlike synthetic tricopper complexes, TNC is embedded in a protein matrix, which provides conformational strains and site isolation that reduce reorganization energy during electron transfer (ET).[20,21] According to Marcus theory, electron transfer in solution is strongly influenced by both inner

Department of Chemistry and Biochemistry, The Ohio State University, 100 W. 18th Ave, Columbus, OH, USA. E-mail: zhang.8941@osu.edu

† Electronic supplementary information (ESI) available: Experimental details, theoretical calculations, and supporting figures. CCDC 1987932 and 1984893–1984895. For ESI and crystallographic data in CIF or other electronic format see DOI: 10.1039/d0sc05441k

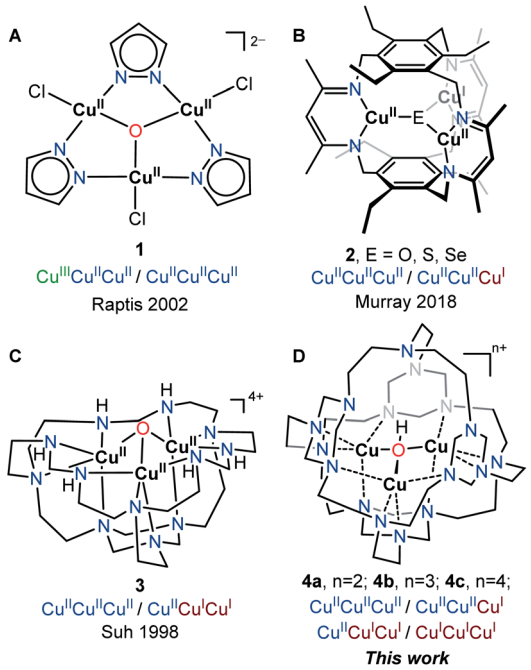

Fig. 1 Redox-active tricopper clusters and their corresponding oxidation states demonstrated by CV study. **1–3** were isolated at one oxidation state. **4** reported in this work is isolated and characterized at three different oxidation states, denoted as **4a**, **4b**, and **4c**.

sphere ligand interactions and outer sphere solvent environments.[17] We posited that the encapsulation of a synthetic tricopper cluster in a cryptand could constrain the coordination environment, hence lowing the barriers for reorganization and allowing access to different redox states of tricopper clusters. Instead of using bulky ligands to simulate the protein environment, we leveraged a multicyclic azacryptand ligand to restrict the conformational freedom and limit solvent interactions. The electrochemical property of **4** was compared to its solvent-exposed analog $[\mathbf{TREN_3}Cu^{II}Cu^{II}Cu^{II}(\mu_3\text{-}O)]Cl_4$, **3**[22] to understand how compartmentalization of tricopper center impacts the redox behavior of Cu^{II}/Cu^{I}.

Results and discussion

The tricopper complex $[\mathbf{TREN_3}Cu^{II}Cu^{II}Cu^{II}(\mu_3\text{-}O)](PF_6)_4$, **3** (Fig. 1C) has been considered as a structural[22] and spectroscopic model[23,24] for TNC. However, **3** does not exhibit the multi-electron redox function of TNC. The *ca.* 550 mV separation of the redox couple (Fig. 4C), which is typical for synthetic tricopper complexes, indicates a substantial barrier for reorganization during ET. Notably, the reduction of $Cu^{II}Cu^{I}Cu^{I}$ to $Cu^{I}Cu^{I}Cu^{I}$ was not observed within the voltage window of water, suggesting **3** is not suitable to activate dioxygen. To construct an isolated microenvironment, we sought to install an additional TREN cap on **3** to afford **4** (Fig. 1D). The desired azacryptand $\mathbf{TREN_4}$ has been synthesized previously,[25] however, no transition metal complex has been reported thus far. We found that metalation of $\mathbf{TREN_4}$ with Cu(I) and Cu(II) salts only afforded complicated mixtures in low yields. Inspired by the metal-templated synthesis reported by Suh *et al.*,[22] we explored the one-pot reaction of copper salts, TREN, and paraformaldehyde. Reaction of $[Cu^{I}(MeCN)_4]PF_6$, TREN (3.3 equivalents), and paraformaldehyde (20 equivalents based on CH_2O units) resulted in the formation of a blue solid (Fig. 2A). Workup and recrystallization under our optimized conditions afforded complex **4b** in 18% yield (see ESI†).

The Electrospray Ionization Mass Spectrum (ESI-MS, Fig. 2B) of **4b** exhibited a prominent peak at 312.2 *m*/*z*, and the isotope distribution pattern matches that of $[\mathbf{TREN_4}Cu^{II}Cu^{I}Cu^{I}(\mu_3\text{-}OH)]^{3+}$ (molecular mass = 938.75 g mol^{-1}, $C_{36}H_{75}Cu_3N_{16}O$), supporting the presence of a $[Cu_3(\mu_3\text{-}OH)]^{3+}$ core. The frozen solution electron paramagnetic resonance (EPR) spectrum of **4b** (Fig. 2C) displayed a rhombic signal ($g_x = 2.25$, $g_y = 2.14$, $g_z = 2.01$) with hyperfine couplings to one $^{63/65}Cu$ ($I = 3/2$) nucleus ($A_z(Cu) = 146$ MHz), suggesting a valence-localized one-hole $Cu^{II}Cu^{I}Cu^{I}$ electronic structure. The high g_x and g_y values indicated that the unpaired electron resides in the d_{z^2} orbital, consistent with a trigonal bipyramidal geometry.[26]

Single crystal X-ray diffraction analysis of **4b** confirmed its assignment as mixed-valent $[\mathbf{TREN_4}Cu^{II}Cu^{I}Cu^{I}(\mu_3\text{-}OH)](PF_6)_3$ (Fig. 3). Cryptate **4b** shares the macrocyclic tricopper assembly of **3** but features a fully encapsulated tricopper core. Three of four TREN moieties in $\mathbf{TREN_4}$ serve as bowl-shape binding sites for the tricopper core, while the remaining one forms a cryptand that isolates the $Cu_3(\mu_3\text{-}OH)$ core in a capsule. With its one-hole $Cu^{II}Cu^{I}Cu^{I}$ oxidation state, complex **4b** is the first synthetic model for the alternative resting (AR) state in MCO ($Cu^{II}Cu^{I}Cu^{I}$).[27,28] The Cu···Cu and Cu–O bond metrics within **4b** (Cu···Cu: 2.973–3.260 Å; Cu–O: 1.878–1.971 Å) are similar to those in **3** (Cu···Cu: 3.095 Å; Cu–O: 1.863 Å) but vary greater from each other, perhaps as a result of its localized electronic structure.

To evaluate the impact of tricopper encapsulation on the redox capability, we performed cyclic voltammetry (CV) studies of **3** and **4** in aqueous environments with pH values range from 5.6 to 13. Dissolution of **3** in water produces an equilibrium mixture of **3** and its conjugate acid ($pK_a = 4.6$).[22] Cyclic voltammogram of **3** at pH = 5.6 showed an irreversible reduction at

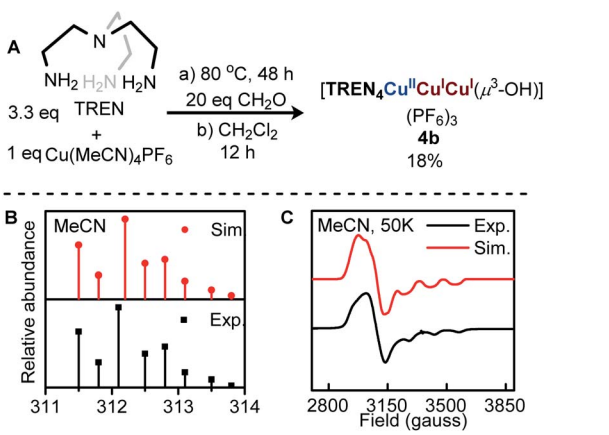

Fig. 2 (A) Synthesis of $[\mathbf{TREN_4}Cu^{II}Cu^{I}Cu^{I}(\mu_3\text{-}OH)](PF_6)_3$ (**4b**). (B) ESI-MS (positive mode) of **4b**, (C) X-band EPR spectrum (frozen MeCN, 0.5 mM) of **4b**, $g_x = 2.25$ $g_y = 2.14$, $g_z = 2.01$, $A_z(Cu) = 146$ MHz.

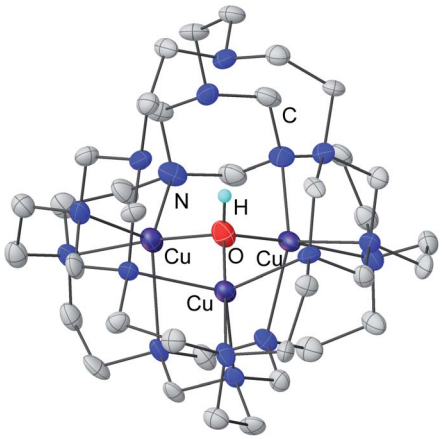

Fig. 3 Solid-state structure of **4b** (100 K) with thermal ellipsoids shown at 35% probability level. All PF_6 anions, the minor components of disorder, and all C–H hydrogen atoms are omitted for clarity.

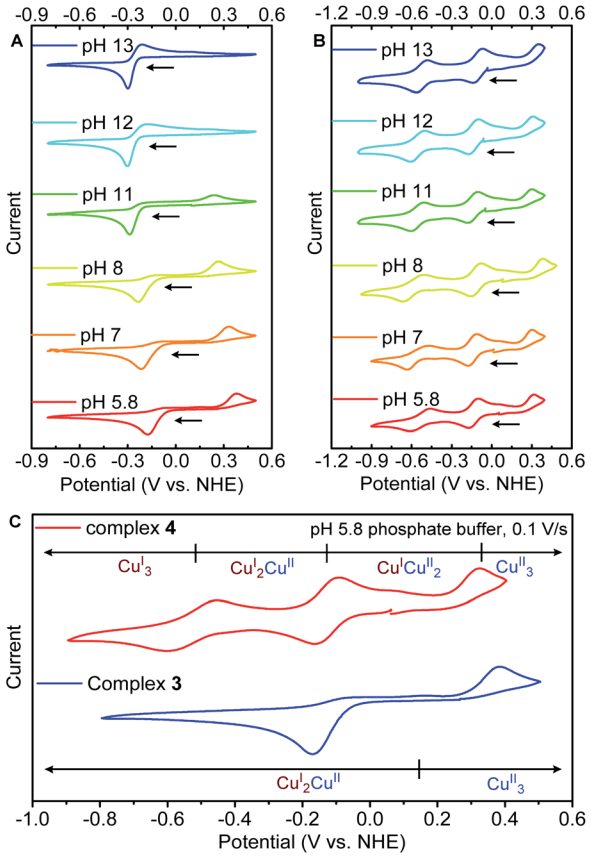

Fig. 4 Cyclic voltammogram of (A) **3** and (B) **4**, in an aqueous environment with various pH from 5.8 to 13 (phosphate buffer solution). (C) Overlay of the CV of **3** and **4** in an aqueous environment with pH = 5.8 (phosphate buffer solution). Scan rate of 0.1 V s^{-1}. Working electrode: glassy carbon; counter electrode: Pt wire; reference electrode: Ag/AgCl.

−0.18 V (*vs.* NHE), which gradually shifts to −0.30 V (*vs.* NHE) at pH = 13. This cathodic peak is assigned to the two-electron reduction of $[Cu^{II}Cu^{II}Cu^{II}(\mu_3\text{-OH})]^{5+}$ to $[Cu^{II}Cu^{I}Cu^{I}(\mu_3\text{-OH})]^{3+}$ based on variable scan rate CV study (see ESI, Fig. S19†). During the reverse scan, an anodic peak was observed at 0.37 V (*vs.* NHE, pH = 5.8), which is attributed to the oxidation of $[Cu^{II}Cu^{I}Cu^{I}(\mu_3\text{-OH})]^{3+}$ back to $[Cu^{II}Cu^{II}Cu^{II}(\mu^3\text{-OH})]^{5+}$ (Fig. 4A). The *ca.* 550 mV separation of the redox couple indicates a substantial geometric difference at $Cu^{II}Cu^{II}Cu^{II}$ and $Cu^{II}Cu^{I}Cu^{I}$ states. As the tricopper center in **3** is exposed to bulk exterior, it can lose/gain interactions with solvents during redox processes, further raising the reorganization energy. Notably, further reduction of $[Cu^{II}Cu^{I}Cu^{I}(\mu_3\text{-OH})]^{3+}$ to $[Cu^{I}Cu^{I}Cu^{I}(\mu_3\text{-OH})]^{2+}$ was not observed within the voltage window of water. The CV of **3** becomes more reversible as the pH increases from 5.6 to 13, perhaps due to the deprotonation of central μ_3-OH to μ_3-O, a stronger ligand that rigidifies the coordination environment (see ESI, Scheme S2†).

In contrast to the irreversible redox behavior of **3**, the cyclic voltammogram of **4** shows two reversible ($E_{1/2}$ = −0.55 V and −0.13 V *vs.* NHE) and one irreversible (E_{ox} = 0.33 V *vs.* NHE) redox events, allowing access to all four oxidation states of the tricopper cluster electrochemically (Fig. 4B). The three redox events of complex **4** are insensitive to the pH of the buffer (Fig. 4B), implicating that the cryptand of **$TREN_4$** isolates the tricopper core from direct solvent interactions. Additionally, the CVs of **4** in aqueous and non-aqueous environments, *e.g.* dimethylformamide (DMF) or acetonitrile, are essentially the same (Fig. S17†), further supporting that the redox of tricopper center in **4** is unaffected by the bulk exterior. As shown in the Fig. 4C, the reduction potentials required to reach $Cu^{II}Cu^{I}Cu^{I}$ state (−0.17 V for **3**, −0.17 V for **4**) and the oxidation potentials required for $Cu^{II}Cu^{II}Cu^{II}$ state (0.38 V for **3**, 0.32 V for **4**) are similar for **3** and **4**. Given the less electron-donating nature of **$TREN_3$** *vs.* **$TREN_4$**, the reduction and oxidation peaks of **3** should be more anodic than those of **4**. The fact that **3** and **4** share the similar redox potentials suggests that the high solvent accessibility of **3** has shifted its redox potentials cathodically. Solvent molecules may serve as ligands to tricopper core and make **3** more electron-rich, while the tricopper core in **4** is completely shielded from such solvent coordination. This is also consistent with the cathodic shift of the reduction and oxidation peak of **3** when the pH of the solvent increases (Fig. 4A).

The highly reversible oxidation and reduction couples of **4b** prompted us to pursue the isolation of fully reduced $[$**$TREN_4$**-$Cu^{I}Cu^{I}Cu^{I}(\mu_3\text{-OH})]^{2+}$ (**4a**, Fig. 5A) and two-hole $[$**$TREN_4$**-$Cu^{II}Cu^{II}Cu^{I}(\mu_3\text{-OH})]^{4+}$ (**4c**, Fig. 5A). Consistent with its electrochemical behavior, chemical oxidation of **4b** with decamethylferrocenium hexafluorophosphate ($Me_{10}FcPF_6$, $E_{1/2}$ = −0.49 V *vs.* Fc^+/Fc) afforded a dark blue compound $[$**$TREN_4$**-$Cu^{II}Cu^{II}Cu^{I}(\mu_3\text{-OH})](PF_6)_4$ (**4c**) in 50% yield (Fig. 5A). ^{1}H NMR spectrum of **4c** shows nineteen broad resonances from 0.13 to 122.5 ppm (see ESI, Fig. S8†), indicating an $S = 1$ ground state. Complex **4c** is a rare example of a tricopper cluster with a $Cu^{II}Cu^{II}Cu^{I}$ oxidation state with the only other example being **2** reported by Murray *et al.*[19] Chemical reduction of **4b** with cobaltocene (Cp_2Co, $E_{1/2}$ = −1.3 V *vs.* Fc^+/Fc) led to a rapid color change from blue to yellow (Fig. 5B), and colorless crystals of

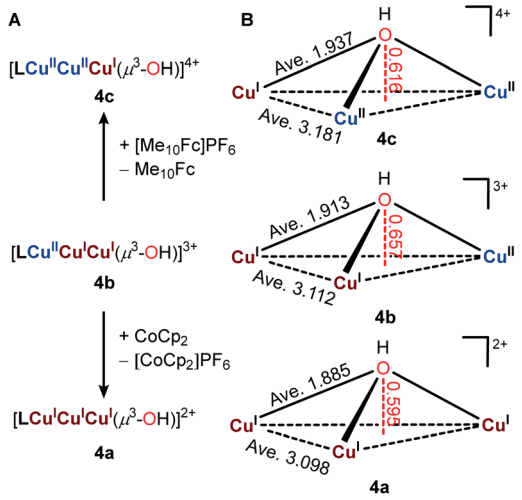

Fig. 5 (A) Synthesis of **4a** and **4c** from **4b**. (B) Geometric comparison of the $Cu_3[\mu_3\text{-O(H)}]$ core in **4a**, **4b**, and **4c**. All bond metrics (Å) were determined based on X-ray single-crystal diffraction.

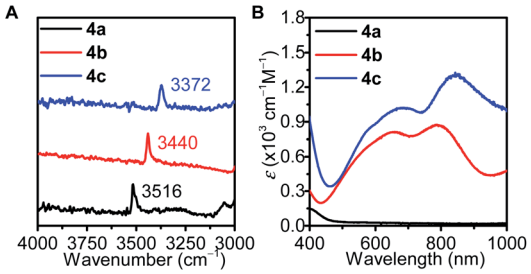

Fig. 6 (A) Infrared and (B) UV-vis spectra of **4a** ($Cu^ICu^ICu^I$, black), **4b** ($Cu^{II}Cu^ICu^I$, red), and **4c** ($Cu^{II}Cu^{II}Cu^I$, blue).

fully reduced $[\mathbf{TREN_4}Cu^ICu^ICu^I(\mu_3\text{-OH})](PF_6)_2$ (**4a**) were obtained by recrystallization. ^{1}H NMR characterization of **4a** was hampered by its low solubility. Therefore, we synthesized an analog of **4a** with (3,5-bis(trifluoromethyl)phenyl)borate (BAr^F_4) counter anions (**4a**-BAr^F_4) by treating **4b**-BAr^F_4 with Cp_2Co. All five ^{1}H NMR resonances of **4a**-BAr^F_4 between 2 to 4.5 ppm are quite broad, perhaps because of the dynamic behavior of CH_2 groups on $\mathbf{TREN_4}$ (see ESI, Fig. S6†).

Both **4a** and **4c** were characterized by X-ray single crystallography (Fig. 5B, S12 and S13†). The geometric features of $Cu_3(\mu_3\text{-OH})$ are maintained throughout the redox processes. Complex **4a** has a slightly contracted $[Cu^ICu^ICu^I(\mu_3\text{-OH})]^{2+}$ core as evidenced by the shortened Cu···Cu distance (average 3.098 Å in **4a** comparing to 3.112 Å in **4b**) and Cu–O distances (average 1.885 Å in **4a** comparing to 1.913 Å in **4b**). In contrast, the $[Cu^{II}Cu^{II}Cu^I(\mu_3\text{-OH})]^{4+}$ core in **4c** expanded (average Cu···Cu distance 3.181 Å, average Cu–O distance 1.937 Å) because of the increased coulombic repulsion. The minimal geometric differences of complex **4a**, **4b**, and **4c** agree with their highly reversible redox behaviors. Importantly, the trigonal bipyramidal geometry of the Cu centers is preserved, even at the $Cu^ICu^ICu^I$ state, highlighting the extraordinary constraints imposed by the multicyclic ligand $\mathbf{TREN_4}$, a feature not shared by $\mathbf{TREN_3}$.

Infrared spectra of complexes **4a**, **4b**, **4c** reveal that the O–H stretches of μ_3-OH progressively blueshifts from 3372 cm^{-1} ($Cu^{II}Cu^{II}Cu^I$) to 3440 cm^{-1} ($Cu^{II}Cu^ICu^I$) to 3516 cm^{-1} ($Cu^ICu^ICu^I$), indicating increasing O–H bond strength as Cu oxidation state decreases (Fig. 6A). The UV-vis spectra of **4b** and **4c** both exhibit two broad intervalence charge-transfer bands (**4b**: 655 nm (800 M^{-1} cm^{-1}) and 790 nm (870 M^{-1} cm^{-1}), **4c**: 680 nm (1000 M^{-1} cm^{-1}) and 850 nm (1300 M^{-1} cm^{-1}), Fig. 6B). Time-dependent density functional theory (TD-DFT) calculations at the TPSSh/TZVP level showed that these absorptions originate from charge transfers from combinations of copper d orbitals to the LUMO, which features the σ* interaction of copper d_{z^2} and the μ_3-O p_z (see ESI, Tables S5 and S6†). Moreover, the calculated UV-vis spectra reflected the red-shifting trend from **4b** to **4c** (see ESI, Fig. S22†).

The reorganization energies (λ) of tricopper clusters during ET have important implications in oxygen reduction reaction catalyzed by MCO.[29] The reorganization energies of TNC have been used to rationalize the various rates of intermolecular ET between type 1 Cu sites and TNC[21] as well as the inhibition[30] or acceleration[31] of ORR by halides. To further understand the kinetic factors that govern the redox of **4**, we evaluated the self-exchange rates (k_{11}) and reorganization energy (λ) of $Cu^ICu^ICu^I$/$Cu^{II}Cu^ICu^I$ and $Cu^{II}Cu^ICu^I$/$Cu^{II}Cu^{II}Cu^I$ redox couples. Determine of k_{11} using ^{1}H NMR line broadening experiment[32] was not feasible due to the dynamic behavior of CH_2 resonances in **4a** and paramagnetic nature of **4c**. As an alternative, we employed an electrochemical method reported by Nicholson;[33,34] the self-exchange rates of **4a**/**4b** and **4b**/**4c** were determined to be 7.4(2) × 10^5 M^{-1} s^{-1} and 7.2(2) × 10^5 M^{-1} s^{-1}, respectively (see ESI, Fig. S20†). These fast ET rates approach the fastest synthetic mono- and dicopper system (10^5 to 10^6 M^{-1} s^{-1})[33,35–43] as well as Nature's blue copper ET protein 10^5 to 10^6 M^{-1} s^{-1}.[44,45] The corresponding reorganization energies for **4a**/**4b** and **4b**/**4c** were calculated to be 1.21(1) eV and 1.21(1) eV using eqn (1) ($Z = 10^{11}$ M^{-1} s^{-1}, $T = 298$ K).[39,46]

$$k_{11} = Z \exp\left(\frac{-\lambda}{4RT}\right) \quad (1)$$

The reorganization energy (λ) can be further partitioned into inner-sphere reorganization energy (λ_i, ligands and coordinated/hydrogen-bonded solvent molecules) and outer-sphere reorganization energy (λ_o, free solvent molecules, eqn (2)). The outer sphere reorganization energy can be estimated with eqn (3), which is based on a spherical model that separates the inner sphere and the outer sphere contribution. Solvent molecules association and dissociation with the inner sphere during the electron transfer will affect the accuracy in the reorganization energy calculation. In order to minimize the inaccuracy in determining the reorganization energy caused by direct hydrogen bonding of solvent with **3** and **4**, acetonitrile was utilized, instead of water, in the electrochemical study and the following calculations. The outersphere reorganization energy was calculated to be 0.68 eV for **4a**/**4b** and **4b**/**4c** using eqn (3), where Δe is the elementary charge, a_1 and a_2 are the radii of redox partners, and D_{opt} and D_{stat} are optical- and static-

Table 1 Inner-sphere reorganization energy (λ_i, eV) of **4** and **3**

	$Cu^{II}Cu^{I}Cu^{I}/Cu^{I}Cu^{I}Cu^{I}$	$Cu^{II}Cu^{II}Cu^{I}/Cu^{II}Cu^{I}Cu^{I}$	$Cu^{II}Cu^{II}Cu^{II}/Cu^{II}Cu^{II}Cu^{I}$
4	0.53(1)[a]	0.53(1)[a]	0.18[b]
	0.70[b]	0.42[b]	
3	2.1[b]	0.68[b]	0.34[b]

[a] Experimental reorganization energies determined by electrochemical measurements. [b] Calculated reorganization energies by DFT.

dielectric constants of acetonitrile[47] at 298.15 K. Thus, the inner-sphere reorganization energy for **4a**/**4b** and **4b**/**4c** are estimated to be 0.53(1) eV and 0.53(1) eV using eqn (2).

$$\lambda = \lambda_i + \lambda_o \quad (2)$$

$$\lambda_o = \Delta e^2 \left[\frac{1}{2a_1} + \frac{1}{2a_2} - \frac{1}{a_1 + a_2}\right]\left[\frac{1}{D_{opt}} - \frac{1}{D_{stat}}\right] \quad (3)$$

$$\lambda_i = \lambda_{ox} + \lambda_{red} \quad (4)$$

Determination of k_{11} of **3** was not viable, since the redox of $Cu^{II}Cu^{II}Cu^{II}/Cu^{II}Cu^{I}Cu^{I}$ was not reversible, and $Cu^{II}Cu^{I}Cu^{I}/Cu^{I}Cu^{I}Cu^{I}$ was not observed experimentally. Therefore, we turned to computational study to compare the reorganization energies of **3** and **4**. The inner-sphere reorganization energy λ_i can be calculated by eqn (4), where λ_{ox} and λ_{red} are the reorganization energy of the reduced and oxidized complexes. λ_{ox} and λ_{red} can be computationally estimated by the energy required to distort the equilibrium geometries to their redox-partners' geometries (see ESI, Fig. S21 and Scheme S3†).[29,30,48]

Single-point energies of **3** and **4** at all four redox states were calculated at TPSSh/def2-TZVP(Cu)/def2-SVP(C, N, O, H) level with a continuum solvation model[49] and dispersion corrections.[50,51] The Gibbs free energy of each species was determined by adding the solvated single point SCF energy to the thermal correction from the respective frequency calculation.[52] The frequency calculations were conducted with BP86 functional due to the conversion issues of a few species in high spin states with other hybrid functionals. There are several competing spin states for the $Cu^{II}Cu^{II}Cu^{II}$ and $Cu^{II}Cu^{II}Cu^{I}$ oxidation states. Since our goal is to compare the reorganization energies of **3** and **4**, we have only studied the electronic states with the lowest energies, that is quartet states for $Cu^{II}Cu^{II}Cu^{II}$ with three ferromagnetically coupled Cu(II) centers and triplet states for $Cu^{II}Cu^{II}Cu^{I}$ with two ferromagnetically coupled Cu(II) centers (see ESI, Table S3†). We compared the optimized geometry of **3** and **4** at different redox states (Table S7 and Fig. S23†). Consistent with their solid-state structure, no significant geometric distortion was observed for **4** at all four oxidation states. In contrast, there was substantial geometric changes of **3** from $Cu^{II}Cu^{I}Cu^{I}$ to $Cu^{I}Cu^{I}Cu^{I}$ state, which may results in large reorganization energy for $Cu^{II}Cu^{I}Cu^{I}/Cu^{I}Cu^{I}Cu^{I}$ couple (Fig. S23†).

The inner-sphere reorganization energies (λ_i) of **3** and **4** were summarized in Table 1 and Scheme S3.† The λ_i values of **3** for each redox couple are generally greater than those of **4**. The especially high λ_i value for $Cu^{II}Cu^{I}Cu^{I}/Cu^{I}Cu^{I}Cu^{I}$ redox couple of **3** (2.1 eV) agrees with the large degree of geometry distortion. Consequently, a large separation between the reduction and oxidation peak may be expected, which explains why the fully reduced $Cu^{I}Cu^{I}Cu^{I}$ state for **3** cannot be achieved within the chemical window of water.[53] The large inner-sphere reorganization energy for $[\mathbf{TREN_3}Cu^{II}Cu^{I}Cu^{I}(\mu_3\text{-}O)]^{2+}/[\mathbf{TREN_3}\text{-}Cu^{I}Cu^{I}Cu^{I}(\mu_3\text{-}O)]^{+}$ (2.1 eV) may be rationalized by its trigonal bipyramidal Cu centers, a geometry highly preferred by Cu(II). As a result, the reduction of $Cu^{II}Cu^{I}Cu^{I}$ to $Cu^{I}Cu^{I}Cu^{I}$, in an unconstrained environment, could be coupled with chemical reactions, *e.g.* ligand dissociation/reorganization. In contrast, multicyclic ligand $\mathbf{TREN_4}$ prevents such ligand dissociation and restrict solvent access to the tricopper centers, synergistically yielding small reorganization energy and fast ET rates.

The generation of the fully reduced $Cu^{I}Cu^{I}Cu^{I}$ state is crucial for oxygen reduction reaction at MCO. Encouraged by the redox capability of **4**, we studied its ability to reduce O_2. As followed by UV-vis spectroscopy (see ESI, Fig. S10†), fully reduced **4a** slowly reduced O_2, while **4b** and **4c** did not react with O_2, consistent with the fact that generation of $Cu^{I}Cu^{I}Cu^{I}$ state is required to harness the oxidative power of O_2. Addition of proton sources, *e.g.* acetic acid, significantly accelerated the rate of ORR. Complex **4b** was regenerated in 96(2)% spectroscopic yield. The product of the O_2 reduction was assigned as H_2O_2 in 97(2)% yield based on iodometric titration (see ESI, Table S1†).[54] To elucidate the mechanism of ORR, we performed the reaction **4a** with $^{18}O_2$ in the presence of acetic acid. The resulting solution of **4b** was analyzed by ESI-MS for ^{18}O incorporation. Spectrum simulations show 10% of ^{18}O incorporation (Fig. S15†), indicating that the ORR most likely proceeds through an outer-sphere mechanism,[55] consistent with the predominant H_2O_2 selectivity.

Conclusions

In conclusion, we report that the encapsulation of tricopper core in a cryptand allows the redox of three Cu^{II}/Cu^{I} to be harnessed effectively in a homogeneous synthetic system. The tricopper complex was isolated and characterized in three of four oxidation states, showing that the redox-induced geometric changes were minimal. The encapsulated tricopper complex has self-exchange ET rates of 10^5 to 10^6 M^{-1} s^{-1}, approaching Nature's copper electron transfer sites (blue copper protein 10^5 to 10^6 M^{-1} s^{-1}). Marcus analysis indicates that the reorganization energy required for the reduction of **4b** to **4a** was 0.70 eV, much smaller than that for solvent-exposed **3** (2.1 eV). These results are particularly consistent with the minimal structural

difference of **4** at $Cu^{I}Cu^{I}Cu^{I}$, $Cu^{II}Cu^{I}Cu^{I}$, and $Cu^{II}Cu^{II}Cu^{I}$ state and suggest that multicyclic cryptands $\mathbf{TREN_4}$ is effective at providing an isolated microenvironment. The geometric constraints and exclusion of solvent interactions synergistically reduce the reorganization energy of electron transfer. At last, we show that the fully reduced $Cu^{I}Cu^{I}Cu^{I}$ cryptate can participate in oxygen reduction reaction. Taken together, our work provides insights into Nature strategy in leveraging the cooperativity of multimetallic sties in multielectron transformation. Our results show that redox processes not operational in bulk solution could potentially be accomplished by full encapsulation of the active site in an isolated environment.

Conflicts of interest

There are no conflicts to declare.

Acknowledgements

We are grateful for financial supports from OSU, ACS-PRF (59036-DNI3), and National Science Foundation (CHE-1904560). The authors thank The Ohio State University Department of Chemistry and Biochemistry for additional financial support. High-performance computing resources were provided by the Ohio Supercomputer Center.

References

1 A. K. Gupta and W. B. Tolman, *Inorg. Chem.*, 2012, **51**, 1881–1888.
2 A. P. Cole, D. E. Root, P. Mukherjee, E. I. Solomon and T. D. P. Stack, *Science*, 1996, **273**, 1848–1850.
3 M. Taki, S. Teramae, S. Nagatomo, Y. Tachi, T. Kitagawa, S. Itoh and S. Fukuzumi, *J. Am. Chem. Soc.*, 2002, **124**, 6367–6377.
4 B. J. Cook, G. N. Di Francesco, M. T. Kieber-Emmons and L. J. Murray, *Inorg. Chem.*, 2018, **57**, 11361–11368.
5 D. Lionetti, M. W. Day and T. Agapie, *Chem. Sci.*, 2013, **4**, 785–790.
6 X. Engelmann, E. R. Farquhar, J. England and K. Ray, *Inorg. Chim. Acta*, 2018, **481**, 159–165.
7 E. Y. Tsui, M. W. Day and T. Agapie, *Angew. Chem., Int. Ed.*, 2011, **50**, 1668–1672.
8 K. D. Karlin, G. Qingfen, A. Farooq, L. Shuncheng and J. Zubieta, *Inorg. Chim. Acta*, 1989, **165**, 37–39.
9 E. C. Brown, B. Johnson, S. Palavicini, B. E. Kucera, L. Casella and W. B. Tolman, *Dalton Trans.*, 2007, 3035–3042.
10 E. I. Solomon, U. M. Sundaram and T. E. Machonkin, *Chem. Rev.*, 2002, **96**, 2563–2606.
11 N. Mano, H.-H. Kim and A. Heller, *J. Phys. Chem. B*, 2002, **106**, 8842–8848.
12 V. C.-C. Wang, S. Maji, P. P.-Y. Chen, H. K. Lee, S. S.-F. Yu and S. I. Chan, *Chem. Rev.*, 2017, **117**, 8574–8621.
13 P. P.-Y. Chen, R. B.-G. Yang, J. C.-M. Lee and S. I. Chan, *Proc. Natl. Acad. Sci. U. S. A.*, 2007, **104**, 14570–14575.
14 S. I. Chan, Y.-J. Lu, P. Nagababu, S. Maji, M.-C. Hung, M. M. Lee, I.-J. Hsu, P. D. Minh, J. C.-H. Lai, K. Y. Ng, S. Ramalingam, S. S.-F. Yu and M. K. Chan, *Angew. Chem., Int. Ed.*, 2013, **52**, 3731–3735.
15 J. Yoon and E. I. Solomon, *Coord. Chem. Rev.*, 2007, **251**, 379–400.
16 E. Salvadeo, L. Dubois and J. Latour, *Coord. Chem. Rev.*, 2018, **374**, 345–375.
17 R. A. Marcus, *J. Chem. Phys.*, 1956, **24**, 966–978.
18 M. Rivera-Carrillo, I. Chakraborty, G. Mezei, R. D. Webster and R. G. Raptis, *Inorg. Chem.*, 2008, **47**, 7644–7650.
19 B. J. Cook, G. N. Di Francesco, R. B. Ferreira, J. T. Lukens, K. E. Silberstein, B. C. Keegan, V. J. Catalano, K. M. Lancaster, J. Shearer and L. J. Murray, *Inorg. Chem.*, 2018, **57**, 11382–11392.
20 S. M. Jones and E. I. Solomon, *Cell. Mol. Life Sci.*, 2015, **72**, 869–883.
21 D. E. Heppner, C. H. Kjaergaard and E. I. Solomon, *J. Am. Chem. Soc.*, 2013, **135**, 12212–12215.
22 M. P. Suh, M. Y. Han, J. H. Lee, K. S. Min and C. Hyeon, *J. Am. Chem. Soc.*, 1998, **120**, 3819–3820.
23 J. Yoon, L. M. Mirica, T. D. P. Stack and E. I. Solomon, *J. Am. Chem. Soc.*, 2005, **127**, 13680–13693.
24 J. Yoon and E. I. Solomon, *Inorg. Chem.*, 2005, **44**, 8076–8086.
25 Z. Bing-Guang, M. Hong, D. Chun-Ying, H. Cheng, M. Qing-Jin, W. Zhe-Ming and Y. Chun-Hua, *Chem. Commun.*, 2001, **24**, 2652–2653.
26 E. Garribba and G. Micera, *J. Chem. Educ.*, 2006, **83**, 1229–1232.
27 C. H. Kjaergaard, S. M. Jones, N. Mano and E. I. Solomon, *J. Am. Chem. Soc.*, 2015, **137**, 8783–8794.
28 C. H. Kjaergaard, F. Durand, F. Tasca, M. F. Qayyum, B. Kauffmann, S. Gounel, E. Suraniti, K. O. Hodgson, B. Hedman, N. Mano and E. I. Solomon, *J. Am. Chem. Soc.*, 2012, **134**, 5548–5551.
29 L. Hu, M. Farrokhnia, J. Heimdal, S. Shleev, L. Rulíšek and U. Ryde, *J. Phys. Chem. B*, 2011, **115**, 13111–13126.
30 K. P. Kepp, *Inorg. Chem.*, 2015, **54**, 476–483.
31 S. Tian, S. M. Jones, A. Jose and E. I. Solomon, *J. Am. Chem. Soc.*, 2019, **141**, 10736–10743.
32 E. W. Dahl and N. K. Szymczak, *Angew. Chem.*, 2016, **128**, 3153–3157.
33 M. Gennari, J. Pécaut, S. DeBeer, F. Neese, M.-N. Collomb and C. Duboc, *Angew. Chem., Int. Ed.*, 2011, **50**, 5662–5666.
34 R. S. Nicholson, *Anal. Chem.*, 1965, **37**, 1351–1355.
35 E. W. Dahl and N. K. Szymczak, *Angew. Chem., Int. Ed.*, 2016, **55**, 3101–3105.
36 H. Doine, Y. Yano and T. W. Swaddle, *Inorg. Chem.*, 1989, **28**, 2319–2322.
37 K. Krylova, C. P. Kulatilleke, M. J. Heeg, C. A. Salhi, L. A. Ochrymowycz and D. B. Rorabacher, *Inorg. Chem.*, 1999, **38**, 4322–4328.
38 E. J. Pulliam and D. R. McMillin, *Inorg. Chem.*, 1984, **23**, 1172–1175.
39 T. J. Zerk, C. T. Saouma, J. M. Mayer and W. B. Tolman, *Inorg. Chem.*, 2019, **58**, 14151–14158.
40 B. Xie, T. Elder, L. J. Wilson, D. M. Stanbury and R. V. August, *Inorg. Chem.*, 1999, **38**, 12–19.

41 B. Xie, L. J. Wilson, D. M. Stanbury and R. V. April, *Inorg. Chem.*, 2001, **40**, 3606–3614.
42 M. Lee, L. Maigre, M. Ibrahim, M. Tahir, E. R. T. Tiekink, T. Begum, R. Rosli, C. Policar, N. Delsuc, K. A. Crouse and J. Pag, *Eur. J. Med. Chem.*, 2016, **120**, 1–12.
43 J. Stanek, M. Konrad, J. Mannsperger, A. Hoffmann and S. Herres-Pawlis, *Eur. J. Inorg. Chem.*, 2018, 4997–5006.
44 C. E. Slutter, R. Langen, D. Sanders, S. M. Lawrence, P. Wittung, A. J. Di Bilio, M. G. Hill, J. A. Fee, J. H. Richards, J. R. Winkler and B. G. Malmström, *Inorg. Chim. Acta*, 1996, **243**, 141–145.
45 E. T. Adman, G. W. Canters, H. A. O. Hill and N. A. Kitchen, *Inorg. Chim. Acta*, 1983, **79**, 127–128.
46 L. E. Eberson, *Electron transfer reactions in organic chemistry*, Springer-Verlag, Berlin, 1987.
47 C. Moreau and D. Gérard, *J. Chem. Thermodyn.*, 1976, **8**, 403–410.
48 E. Sigfridsson, M. H. M. Olsson and U. Ryde, *Inorg. Chem.*, 2001, **40**, 2509–2519.
49 A. V. Marenich, C. J. Cramer and D. G. Truhlar, *J. Phys. Chem. B*, 2009, **113**, 6378–6396.
50 E. R. Johnson and A. D. Becke, *J. Chem. Phys.*, 2006, **124**, 174104.
51 S. Grimme, S. Ehrlich and L. Goerigk, *J. Comput. Chem.*, 2011, **32**, 1456–1465.
52 S. J. Koepke, K. M. Light, P. E. Vannatta, K. M. Wiley and M. T. Kieber-Emmons, *J. Am. Chem. Soc.*, 2017, **139**, 8586–8600.
53 M. C. Henstridge, E. Laborda, N. V. Rees and R. G. Compton, *Electrochim. Acta*, 2012, **84**, 12–20.
54 I. Garcia-Bosch, R. E. Cowley, D. E. Díaz, M. A. Siegler, W. Nam, E. I. Solomon and K. D. Karlin, *Chem.–Eur. J.*, 2016, **22**, 5133–5137.
55 M. L. Pegis, C. F. Wise, D. J. Martin and J. M. Mayer, *Chem. Rev.*, 2018, **118**, 2340–2391.